

Improved Measurements of Branching Fractions and CP Partial Rate Asymmetries for $B \rightarrow \omega K$ and $B \rightarrow \omega \pi$

C.-M. Jen,²⁶ P. Chang,²⁶ K. Abe,⁸ K. Abe,⁴³ I. Adachi,⁸ H. Aihara,⁴⁵ D. Anipko,¹ K. Arinstein,¹ V. Aulchenko,¹ A. M. Bakich,⁴⁰ E. Barberio,²¹ M. Barbero,⁷ A. Bay,¹⁸ I. Bedny,¹ K. Belous,¹² U. Bitenc,¹⁴ I. Bizjak,¹⁴ A. Bondar,¹ A. Bozek,²⁷ M. Bračko,^{8,20,14} T. E. Browder,⁷ A. Chen,²⁴ W. T. Chen,²⁴ B. G. Cheon,³ S.-K. Choi,⁶ Y. Choi,³⁹ Y. K. Choi,³⁹ A. Chuvikov,³⁵ S. Cole,⁴⁰ J. Dalseno,²¹ M. Dash,⁴⁹ A. Drutskoy,⁴ S. Eidelman,¹ D. Epifanov,¹ S. Fratina,¹⁴ N. Gabyshev,¹ T. Gershon,⁸ A. Go,²⁴ G. Gokhroo,⁴¹ B. Golob,^{19,14} H. Ha,¹⁶ J. Haba,⁸ T. Hara,³² K. Hayasaka,²² H. Hayashii,²³ M. Hazumi,⁸ D. Heffernan,³² Y. Hoshi,⁴³ S. Hou,²⁴ W.-S. Hou,²⁶ Y. B. Hsiung,²⁶ T. Iijima,²² K. Inami,²² A. Ishikawa,⁴⁵ R. Itoh,⁸ M. Iwasaki,⁴⁵ Y. Iwasaki,⁸ J. H. Kang,⁵⁰ P. Kapusta,²⁷ N. Katayama,⁸ H. Kawai,² T. Kawasaki,²⁹ H. R. Khan,⁴⁶ H. Kichimi,⁸ H. J. Kim,¹⁷ Y. J. Kim,⁵ P. Križan,^{19,14} P. Krokovny,⁸ R. Kulasiri,⁴ R. Kumar,³³ C. C. Kuo,²⁴ A. Kuzmin,¹ Y.-J. Kwon,⁵⁰ G. Leder,¹¹ S. E. Lee,³⁸ Y.-J. Lee,²⁶ T. Lesiak,²⁷ S.-W. Lin,²⁶ D. Liventsev,¹³ F. Mandl,¹¹ T. Matsumoto,⁴⁷ S. McOnie,⁴⁰ W. Mitaroff,¹¹ H. Miyake,³² H. Miyata,²⁹ Y. Miyazaki,²² T. Nagamine,⁴⁴ Y. Nagasaka,⁹ E. Nakano,³¹ M. Nakao,⁸ Z. Natkaniec,²⁷ S. Nishida,⁸ O. Nitoh,⁴⁸ T. Nozaki,⁸ S. Ogawa,⁴² T. Ohshima,²² S. Okuno,¹⁵ Y. Onuki,²⁹ H. Ozaki,⁸ H. Palka,²⁷ C. W. Park,³⁹ H. Park,¹⁷ L. S. Peak,⁴⁰ R. Pestotnik,¹⁴ L. E. Piilonen,⁴⁹ A. Poluektov,¹ Y. Sakai,⁸ T. Schietinger,¹⁸ O. Schneider,¹⁸ A. J. Schwartz,⁴ R. Seidl,^{10,36} M. E. Sevier,²¹ M. Shapkin,¹² H. Shibuya,⁴² B. Shwartz,¹ A. Somov,⁴ N. Soni,³³ S. Stanič,³⁰ H. Stoeck,⁴⁰ T. Sumiyoshi,⁴⁷ F. Takasaki,⁸ K. Tamai,⁸ M. Tanaka,⁸ G. N. Taylor,²¹ Y. Teramoto,³¹ X. C. Tian,³⁴ T. Tsukamoto,⁸ S. Uehara,⁸ T. Uglov,¹³ S. Uno,⁸ P. Urquijo,²¹ Y. Usov,¹ G. Varner,⁷ K. E. Varvell,⁴⁰ S. Villa,¹⁸ C. C. Wang,²⁶ C. H. Wang,²⁵ M.-Z. Wang,²⁶ Y. Watanabe,⁴⁶ E. Won,¹⁶ A. Yamaguchi,⁴⁴ Y. Yamashita,²⁸ M. Yamauchi,⁸ L. M. Zhang,³⁷ Z. P. Zhang,³⁷ V. Zhilich,¹ and A. Zupanc¹⁴

(The Belle Collaboration)

¹*Budker Institute of Nuclear Physics, Novosibirsk*

²*Chiba University, Chiba*

³*Chonnam National University, Kwangju*

⁴*University of Cincinnati, Cincinnati, Ohio 45221*

⁵*The Graduate University for Advanced Studies, Hayama, Japan*

⁶*Gyeongsang National University, Chinju*

⁷*University of Hawaii, Honolulu, Hawaii 96822*

⁸*High Energy Accelerator Research Organization (KEK), Tsukuba*

⁹*Hiroshima Institute of Technology, Hiroshima*

¹⁰*University of Illinois at Urbana-Champaign, Urbana, Illinois 61801*

¹¹*Institute of High Energy Physics, Vienna*

¹²*Institute of High Energy Physics, Protvino*

¹³*Institute for Theoretical and Experimental Physics, Moscow*

¹⁴*J. Stefan Institute, Ljubljana*

¹⁵*Kanagawa University, Yokohama*

¹⁶*Korea University, Seoul*

¹⁷*Kyungpook National University, Taegu*

¹⁸*Swiss Federal Institute of Technology of Lausanne, EPFL, Lausanne*

¹⁹*University of Ljubljana, Ljubljana*

²⁰*University of Maribor, Maribor*

²¹*University of Melbourne, Victoria*

²²*Nagoya University, Nagoya*

²³*Nara Women's University, Nara*

²⁴*National Central University, Chung-li*

²⁵*National United University, Miao Li*

²⁶*Department of Physics, National Taiwan University, Taipei*

²⁷*H. Niewodniczanski Institute of Nuclear Physics, Krakow*

²⁸*Nippon Dental University, Niigata*

²⁹*Niigata University, Niigata*

³⁰*University of Nova Gorica, Nova Gorica*

³¹*Osaka City University, Osaka*

³²*Osaka University, Osaka*

³³*Panjab University, Chandigarh*

- ³⁴*Peking University, Beijing*
³⁵*Princeton University, Princeton, New Jersey 08544*
³⁶*RIKEN BNL Research Center, Upton, New York 11973*
³⁷*University of Science and Technology of China, Hefei*
³⁸*Seoul National University, Seoul*
³⁹*Sungkyunkwan University, Suwon*
⁴⁰*University of Sydney, Sydney NSW*
⁴¹*Tata Institute of Fundamental Research, Bombay*
⁴²*Toho University, Funabashi*
⁴³*Tohoku Gakuin University, Tagajo*
⁴⁴*Tohoku University, Sendai*
⁴⁵*Department of Physics, University of Tokyo, Tokyo*
⁴⁶*Tokyo Institute of Technology, Tokyo*
⁴⁷*Tokyo Metropolitan University, Tokyo*
⁴⁸*Tokyo University of Agriculture and Technology, Tokyo*
⁴⁹*Virginia Polytechnic Institute and State University, Blacksburg, Virginia 24061*
⁵⁰*Yonsei University, Seoul*

We report improved measurements of B to pseudoscalar-vector decays containing an ω meson in the final states. Our results are obtained from a data sample that contains $388 \times 10^6 B\bar{B}$ pairs accumulated at the $\Upsilon(4S)$ resonance, with the Belle detector at the KEKB asymmetric energy e^+e^- collider. We measure the following branching fractions: $\mathcal{B}(B^+ \rightarrow \omega K^+) = [8.1 \pm 0.6(\text{stat.}) \pm 0.6(\text{syst.})] \times 10^{-6}$, $\mathcal{B}(B^+ \rightarrow \omega\pi^+) = [6.9 \pm 0.6(\text{stat.}) \pm 0.5(\text{syst.})] \times 10^{-6}$, and $\mathcal{B}(B^0 \rightarrow \omega K^0) = [4.4^{+0.8}_{-0.7}(\text{stat.}) \pm 0.4(\text{syst.})] \times 10^{-6}$. The partial width ratio $\frac{\Gamma(B^+ \rightarrow \omega K^+)}{\Gamma(B^0 \rightarrow \omega K^0)} = 1.8 \pm 0.4(\text{stat.}) \pm 0.1(\text{sys.})$. We also set the 90% confidence level upper limit $\mathcal{B}(B^0 \rightarrow \omega\pi^0) < 2.0 \times 10^{-6}$. In addition, we obtain the partial rate asymmetries $\mathcal{A}_{CP} = 0.05^{+0.08}_{-0.07}(\text{stat.}) \pm 0.01(\text{syst.})$ for $B^+ \rightarrow \omega K^+$, and $\mathcal{A}_{CP} = -0.02 \pm 0.09(\text{stat.}) \pm 0.01(\text{syst.})$ for $B^+ \rightarrow \omega\pi^+$.

PACS numbers: 13.30.Er, 11.30.Hv, 13.20.Hv, 13.25.Hw, 14.40.Nd, 14.65.Fy

Charmless hadronic B decays provide a rich ground to understand the dynamics of B meson decays and the origin of CP violation. Two-body B decays with a vector meson and a pseudoscalar particle h (h is either a kaon or a pion) proceed through combinations of color-allowed (T_u) and color-suppressed (C_u) $b \rightarrow u$ tree diagrams and $b \rightarrow s$ (P_s) or $b \rightarrow d$ (P_d) penguin diagrams. For example, $B^+ \rightarrow \omega K^+$ proceeds through T_u , C_u and P_s , $B^0 \rightarrow \omega K^0$ proceeds through P_s , $B^+ \rightarrow \omega\pi^+$ proceeds through T_u , C_u and P_d , and $B^0 \rightarrow \omega\pi^0$ proceeds through C_u and P_d . The QCD factorization (QCDF) approach suggests that the branching fractions of $B^+ \rightarrow \omega h^+$ decays are in the range 10^{-6} – 10^{-5} [1]. The predicted $\mathcal{B}(B^0 \rightarrow \omega K^0)$ and $\mathcal{B}(B^+ \rightarrow \omega K^+)$ are enhanced after including the rescattering effect from final-state interactions [2]. The perturbative QCD (PQCD) approach, on the other hand, suggests that $\mathcal{B}(B^+ \rightarrow \omega K^+) = 3.22 \times 10^{-6}$, and $\mathcal{B}(B^0 \rightarrow \omega K^0) = 2.07 \times 10^{-6}$, and that $\mathcal{B}(B^+ \rightarrow \omega K^+) = (10.6^{+10.4(+7.2)}_{-5.8(-4.4)}) \times 10^{-6}$, and $\mathcal{B}(B^0 \rightarrow \omega K^0) = (9.8^{+8.6(+6.7)}_{-4.9(-4.3)}) \times 10^{-6}$ after considering next-to-leading-order accuracy [3]. Due to the lack of T_u and P_s diagrams, $B^0 \rightarrow \omega\pi^0$ is expected to be small [1, 4]. Experimentally, clear signals have been observed for $B^+ \rightarrow \omega K^+$, $B^+ \rightarrow \omega\pi^+$, and $B^0 \rightarrow \omega K^0$ with similar branching fractions [5, 6, 7]. However, experimental measurements to date are not yet precise enough for a quantitative confirmation of the pattern predicted by QCDF or PQCD.

In this paper, we report improved measurements of branching fractions and partial rate asymmetries for $B \rightarrow \omega h$ decays, where h can be a kaon or pion. The partial rate asymmetry (\mathcal{A}_{CP}) is measured for the charged B decays and defined to be

$$\mathcal{A}_{CP} \equiv \frac{\Gamma(B^- \rightarrow \omega h^-) - \Gamma(B^+ \rightarrow \omega h^+)}{\Gamma(B^- \rightarrow \omega h^-) + \Gamma(B^+ \rightarrow \omega h^+)}. \quad (1)$$

These measurements are based on a data sample of $388 \times 10^6 B\bar{B}$ pairs collected with the Belle detector at the KEKB [8] asymmetric-energy e^+e^- collider. They improve upon our previously published results [5] by a five-fold increase in statistics and supersede them. The Belle detector is a large-solid-angle magnetic spectrometer that consists of a silicon vertex detector (SVD), a 50-layer central drift chamber (CDC), an array of aerogel threshold Čerenkov counters (ACC), a barrel-like arrangement of time-of-flight scintillation counters (TOF), and an electromagnetic calorimeter (ECL) comprised of CsI(Tl) crystals located inside a superconducting solenoid coil that provides a 1.5 T magnetic field. An iron flux-return located outside of the coil is instrumented to detect K_L^0 mesons and to identify muons (KLM). The detector is described in detail elsewhere [9]. In August 2003, the three-layer SVD was replaced by a four-layer radiation tolerant device. The data sample for this analysis consists of 140 fb^{-1} of data recorded with a three-layer SVD (Set I) [9] and 217 fb^{-1} recorded with a four-layer SVD (Set II) [10].

Hadronic events are selected using criteria based on the charged track multiplicity and total visible energy, with an efficiency greater than 99% for generic $B\bar{B}$ events. All primary charged tracks must satisfy quality requirements based on their impact parameters relative to the run-dependent interaction point (IP). For tracks from the candidate B mesons, their deviations from the IP position are required to be within ± 0.1 cm in the transverse direction and ± 3.0 cm in the longitudinal direction.

Charged particle identification is performed using a K - π likelihood ratio, $\mathcal{R}_K = \mathcal{L}_K / (\mathcal{L}_\pi + \mathcal{L}_K)$, where \mathcal{L}_K (\mathcal{L}_π) is the likelihood for a charged particle to be a kaon (pion) based on information from the ACC, TOF and CDC. Charged tracks with $\mathcal{R}_K > 0.6$ are identified as kaons, and tracks with $\mathcal{R}_K < 0.4$ are identified as pions. With these criteria, kaons produced in $B^+ \rightarrow \omega K^+$ decays are selected with an efficiency of 85%, while the corresponding rate of kaons that are misidentified as pions is 11%. On the other hand, pions from $B^+ \rightarrow \omega\pi^+$ are selected with an efficiency of 90% and have a corresponding kaon misidentification rate of 9%.

Candidate π^0 mesons are reconstructed from pairs of photons with an invariant mass in the range of $118 \text{ MeV}/c^2 < M_{\gamma\gamma} < 150 \text{ MeV}/c^2$ (within $\pm 2.5\sigma$ around the PDG value [11]). The cosine of the decay angle should satisfy $|\cos\theta_\gamma| < 0.9$, where θ_γ is the angle between the photon decay axis and the negative of the laboratory frame direction in the π^0 rest frame. Candidate K_S^0 mesons are reconstructed using pairs of oppositely charged tracks that have an invariant mass in the range of $482 \text{ MeV}/c^2 < M_{\pi^+\pi^-} < 514 \text{ MeV}/c^2$ (within $\pm 4\sigma$ around the PDG value [11]). The vertex of the K_S^0 candidate is required to be well reconstructed and displaced from the IP, and the K_S^0 momentum direction must be consistent with the K_S^0 flight direction. Candidate $\omega \rightarrow \pi^+\pi^-\pi^0$ decays are reconstructed from charged tracks with $\mathcal{R}_K < 0.9$ (this requirement has a 96% efficiency per track), and from π^0 candidates with e^+e^- center-of-mass frame (CM) momenta greater than $0.35 \text{ GeV}/c^2$. Candidate ω mesons are required to have invariant masses within $\pm 30 \text{ MeV}/c^2$ ($\sim \pm 3\sigma$) of the PDG value [11].

B meson candidates are formed by combining an ω meson with either a kaon (K^+ , K_S^0) or a pion (π^+ , π^0). Two kinematic variables are used to select B candidates: the beam-energy constrained mass $M_{bc} = \sqrt{(E_{\text{beam}}^{\text{CM}})^2 - |P_B^{\text{CM}}|^2}$, and the energy difference $\Delta E = E_B^{\text{CM}} - E_{\text{beam}}^{\text{CM}}$, where E_B^{CM} is the beam energy in the CM frame, and P_B^{CM} , E_B^{CM} are the momentum and energy, respectively, of the B candidate in the CM frame. Candidates with $M_{bc} > 5.2 \text{ GeV}/c^2$ and $|\Delta E| < 0.25 \text{ GeV}$ ($|\Delta E| < 0.30 \text{ GeV}$ for $B^0 \rightarrow \omega\pi^0$) are selected for further analysis.

The dominant background arises from quark-antiquark continuum events ($e^+e^- \rightarrow q\bar{q}$, $q = u, d, s, c$). The contin-

uum background is characterized by a jet-like structure, while the $B\bar{B}$ events have a more spherical distribution. The following event-shape variables calculated in the CM frame are employed to suppress the continuum. The thrust angle θ_T is defined as the angle between the thrust axis [12] of the B candidate daughter particles and that of the rest of the particles in an event. Signal events are uniformly distributed in $\cos\theta_T$, while continuum events are sharply peaked near $\cos\theta_T = \pm 1.0$. Events with $|\cos\theta_T| < 0.9$ are selected.

A Fisher discriminant is formed by combining a set of modified Fox-Wolfram moments [13] with the variable S_\perp [14]. This variable is the scalar sum of the transverse momenta of particles outside a 45° cone around the B thrust axis, divided by the scalar sum of their momenta. Here, the transverse momenta are calculated with respect to the thrust axis, and we do not include daughters of the B candidate. Further variables that have been found to separate signal from continuum background include: the cosine of the angle between the flight direction of the B candidate and the beam direction ($\cos\theta_B$); the distance along the beam direction between the B vertex and the vertex of the remaining particles in the event (Δz); and the cosine of the helicity angle, defined as the angle between the negative B flight direction in the ω rest frame and the direction normal to the plane defined by the three daughter pions of the ω . The probability density functions (PDFs) for these three variables and the Fisher discriminant are obtained using Monte Carlo (MC) simulation for signal events and sideband data ($M_{bc} < 5.26 \text{ GeV}/c^2$) for $q\bar{q}$ backgrounds. These variables are combined to form a likelihood ratio $\mathcal{R} = \frac{\mathcal{L}_S}{\mathcal{L}_S + \mathcal{L}_{q\bar{q}}}$, where $\mathcal{L}_{S(q\bar{q})}$ is the product of signal ($q\bar{q}$) PDFs.

Additional background discrimination is provided by the quality of the B flavor tagging of the accompanying B meson. We use the standard Belle B tagging package [15], which gives two outputs: a discrete variable (q) indicating the B flavor, and a dilution factor (r) ranging from zero for no flavor information to unity for unambiguous flavor assignment. We divide the data into six r regions. Continuum suppression is achieved by applying a mode-dependent requirement on \mathcal{R} for events in each r region based on the figure-of-merit: $\mathcal{N}_s / \sqrt{\mathcal{N}_s + \mathcal{N}_{q\bar{q}}}$, where \mathcal{N}_s is the expected number of signal events estimated from simulation and our previously published branching fractions [5], and $\mathcal{N}_{q\bar{q}}$ is the number of background events estimated from sideband data ($M_{bc} < 5.26 \text{ GeV}/c^2$). This \mathcal{R} requirement retains 74%, 68%, 74%, and 57% of the signal while rejecting 91%, 94%, 91%, and 95% of the continuum background for the ωK^+ , $\omega\pi^+$, ωK^0 , and $\omega\pi^0$ modes, respectively.

Simulation studies indicate small backgrounds from generic $b \rightarrow c$ transitions in the charged B modes; they are found to be negligible for the neutral modes. Two additional backgrounds have also been considered: re-

reflections of $B \rightarrow \omega\pi^+$ decays due to $\pi^- \rightarrow K$ misidentification, and feed-down from other charmless B decays, predominantly $B \rightarrow \omega K^*(892)$ and $B \rightarrow \omega\rho(770)$. We include these three components in the fit used to extract the signal.

The signal yields and partial rate asymmetries are obtained using an extended unbinned maximum likelihood fit for M_{bc} and ΔE . The likelihood is defined as

$$\mathcal{L} = e^{-\sum_j \mathcal{N}_j} \times \prod_i \left(\sum_j \mathcal{N}_j \mathcal{P}_j \right) \quad (2)$$

$$\mathcal{P}_j = \frac{1}{2} [1 - Q_i \cdot \mathcal{A}_{CPj}] P_j(M_{bci}, \Delta E_i), \quad (3)$$

where i is the identifier of the i -th event, $P_j(M_{bci}, \Delta E_i)$ is the PDF of M_{bc} and ΔE , Q indicates the B meson charge, \mathcal{N}_j is the number of events for category j , which corresponds to either signal, $q\bar{q}$ background, reflections due to K - π misidentification, or $B\bar{B}$ background ($b \rightarrow c$ and charmless). For the neutral B modes, $\mathcal{P}_j = P_j(M_{bci}, \Delta E_i)$, and there is no reflection component or $b \rightarrow c$ background.

The signal distribution in M_{bc} is parameterized by a Gaussian function centered near the mass of the B meson, while the Crystal Ball line shape [16] is used to model the ΔE distribution. Both functions are calibrated with large control samples of $B \rightarrow \bar{D}^0\pi$, $\bar{D}^0 \rightarrow K^+\pi^-\pi^0$, and $B \rightarrow \eta'K$, $\eta' \rightarrow \eta\pi^+\pi^-$, $\eta \rightarrow \gamma\gamma$ decays. The continuum PDF is the product of a first-order polynomial for ΔE and an ARGUS function [17] for M_{bc} . Other background PDFs are modelled by a smoothed two-dimensional $M_{bc} - \Delta E$ function obtained from MC simulation. The yields of the $B\bar{B}$ background mentioned in the previous paragraph are fixed with $\mathcal{A}_{CP} = 0$ in the fit, except for the reflection component. The \mathcal{A}_{CP} and the normalizations of the reflection components are fixed to expectations based on the $B^+ \rightarrow \omega K^+$ and $B^+ \rightarrow \omega\pi^+$ partial rate asymmetries and branching fractions, as well as $K^+ \leftrightarrow \pi^+$ fake rates. The reflection yield and \mathcal{A}_{CP} are calculated according to our measured results.

Figure 1 shows the data and fit results for each mode. Table I lists the resulting event yields, efficiencies, corresponding branching fractions and \mathcal{A}_{CP} . These new results are consistent with those measured by BaBar [7]. The branching fractions are computed as the sum of the yields divided by the corresponding efficiencies in each dataset and the total number of B mesons. The reconstruction efficiency for each mode includes all intermediate branching fractions and is defined as the fraction of the signal yield remaining after all selection criteria, where the yield is determined by performing the unbinned maximum likelihood fit on a MC sample. Small correction factors are included to account for differences in the reconstruction efficiency between MC and data. The correction factor is obtained as a result of the relative

π^0 reconstruction (1.00 for Set I and 0.96 for Set II) using the inclusive $\bar{D}^0 \rightarrow K^+\pi^-$ and $\bar{D}^0 \rightarrow K^+\pi^-\pi^0$ samples. The corresponding systematic error is 4%. We determine the identification efficiency of charged kaons and pions by studying an inclusive $D^{*-} \rightarrow \bar{D}^0\pi^-$, $\bar{D}^0 \rightarrow K^+\pi^-$ sample. This selection criterion leads to a correction factor within the range of 0.90–0.96 and a corresponding systematic error of 1.7% for charged modes and 0.9% for neutral modes. We define the significance as $\sqrt{-2\ln(\mathcal{L}_0/\mathcal{L}_{\max})}$, where \mathcal{L}_{\max} is the maximum likelihood from the fit when the signal branching fraction is floated, and \mathcal{L}_0 is the likelihood obtained when the signal branching fraction is set to zero. The 90% C.L. upper limit for $\mathcal{B}(B^0 \rightarrow \omega\pi^0)$ is calculated using the procedure of Ref. [18], which is based on the Feldman-Cousins method [19]. This procedure accounts for systematic uncertainties (discussed below).

The main systematic uncertainties for the branching fraction measurements are listed in Table II. These are evaluated as follows: charged tracking efficiency (1.0% per track) from partially reconstructed $D^{*+} \rightarrow D^0\pi^+$, $D^0 \rightarrow K^-\pi^+$; K_S^0 reconstruction (4.9%) from $D^+ \rightarrow K_S^0\pi^+$, $D^+ \rightarrow K^-\pi^+\pi^+$; ω mass resolution (3.0%); the requirement on \mathcal{R} (3.0%) from $B^- \rightarrow D^0\pi^-$, $D^0 \rightarrow K^-\pi^+$; MC statistics (1.1–2.4%), and the number of $B\bar{B}$ events in the data samples (1.3%). For the \mathcal{A}_{CP} measurement, the dominant systematic uncertainty comes from the fit parameters. Systematic uncertainties due to fit parameters are evaluated by varying each parameter by $\pm 1\sigma$ and adding in quadrature the resulting deviations from the central value. The total systematic uncertainty is the quadratic sum of all the above contributions. The significance Σ_{sig} listed in Table I includes the total systematic uncertainty.

While the branching fractions for $B^+ \rightarrow \omega K^+$, $B^0 \rightarrow \omega K^0$, and $B^+ \rightarrow \omega\pi^+$ are of comparable size, that for $B^0 \rightarrow \omega\pi^0$ is much smaller as compared to that for $B^+ \rightarrow \omega\pi^+$. This is in agreement with both QCDF and PQCD pictures, which predict that only color-suppressed tree and penguin diagrams contribute to $B^0 \rightarrow \omega\pi^0$ [1, 3, 4]. We also determine the partial width ratio

$$\frac{\Gamma(B^+ \rightarrow \omega K^+)}{\Gamma(B^0 \rightarrow \omega K^0)} = 1.8 \pm 0.4(\text{stat.}) \pm 0.1(\text{sys.}), \quad (4)$$

where the ratio of B meson lifetimes $\frac{\tau_{B^+}}{\tau_{B^0}}$ is taken to be 1.076 ± 0.008 [11]. The systematic error of the partial width ratio is reduced because of the cancellation of several common systematic errors. No evidence for direct CP violation is found for either $B^+ \rightarrow \omega K^+$ or $B^+ \rightarrow \omega\pi^+$.

We thank the KEKB group for the excellent operation of the accelerator, the KEK cryogenics group for the efficient operation of the solenoid, and the KEK computer group and the NII for valuable computing and SuperSINET network support. We acknowledge support from

TABLE I: Signal efficiency (ϵ), signal yield (\mathcal{N}_s), significance including systematic error ($\Sigma_{\text{sig.}}$), branching fraction (\mathcal{B}), the 90% C.L. upper limit (U.L.) and partial rate asymmetry (\mathcal{A}_{CP}) for the $B^+ \rightarrow \omega h^+$ decays. The first and second errors are statistical and systematic, respectively.

Mode	ϵ (%)	\mathcal{N}_s	$\Sigma_{\text{sig.}}$	\mathcal{B} (10^{-6})	U.L. (10^{-6})	\mathcal{A}_{CP}
ωK^+	8.27 ± 0.17	$259.5^{+20.4}_{-19.4}$	19.5σ	$8.1 \pm 0.6 \pm 0.6$	—	$0.05^{+0.08}_{-0.07} \pm 0.01$
$\omega\pi^+$	8.43 ± 0.17	$224.8^{+20.3}_{-19.3}$	17.1σ	$6.9 \pm 0.6 \pm 0.5$	—	$-0.02 \pm 0.09 \pm 0.01$
ωK^0	2.50 ± 0.09	$41.5^{+8.0}_{-7.0}$	9.3σ	$4.4^{+0.8}_{-0.7} \pm 0.4$	—	—
$\omega\pi^0$	3.80 ± 0.12	$5.9^{+4.8}_{-4.1}$	1.5σ	$0.5^{+0.4}_{-0.3} \pm 0.1$	2.0	—

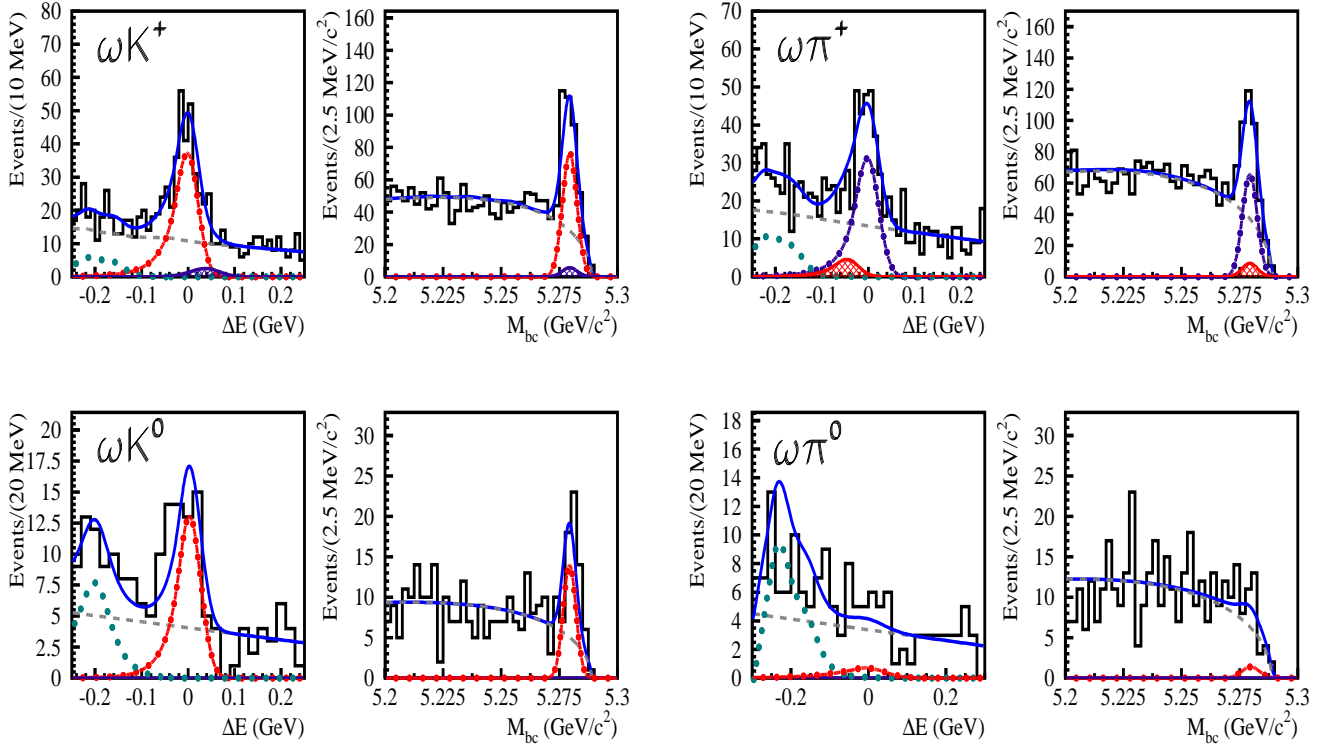


FIG. 1: Projections of fit results on M_{bc} (within the region of $|\Delta E| \leq 0.1$ GeV, $-0.15 \leq \Delta E \leq 0.1$ GeV for $\omega\pi^0$) and ΔE (within the region of $5.27 \text{ GeV}/c^2 < M_{bc} < 5.29 \text{ GeV}/c^2$) for ωK^+ , $\omega\pi^+$, ωK^0 , and $\omega\pi^0$. Open histograms are data, solid curves are the fit functions, solid-dotted lines represent the signals, dashed lines show the sum of $q\bar{q}$ continuum and $b \rightarrow c$, dotted lines are due to other charmless B decays, and cross-hatched areas represent reflections due to $K-\pi$ misidentification.

MEXT and JSPS (Japan); ARC and DEST (Australia); NSFC (contract No. 10175071 China); DST (India); the BK21 program of MOEHRD and the CHEP SRC program of KOSEF (Korea); KBN (contract No. 2P03B 01324, Poland); MIST (Russia); MHEST (Slovenia); SNSF (Switzerland); NSC and MOE (Taiwan); and DOE (USA). C.-M. Jen thanks Y.Y. Chang, H.Y. Cheng, C.H. Chen, C.K. Chua, and H.n. Li for invaluable instruction and discussions on particle physics phenomenology while at AS (Taiwan).

-
- [1] M. Beneke, M. Neubert, Nucl. Phys. B **675**, 333 (2003).
 - [2] H.-Y. Cheng, C.-K. Chua, Amarjit Soni, Phys. Rev. D **72**, 014006 (2005).
 - [3] H.-n. Li, Satoshi Mishima, hep-ph/0608277; C.-H. Chen, Phys. Lett. B **525**, 56 (2002).
 - [4] Cai-Dian Lü, Mao-Zhi Yang, Eur. Phys. J. C **23**, 275 (2002).
 - [5] C.-H. Wang *et al.* (Belle Collab.), Phys. Rev. D **70**, 012001 (2004).
 - [6] B. Aubert *et al.* (BaBar Collab.), Phys. Rev. Lett. **92**, 061801 (2004).
 - [7] B. Aubert *et al.* (BaBar Collab.), Phys. Rev. D(RC) **74**,

TABLE II: systematic uncertainties for ωK and $\omega\pi$ (%).

Mode	ωK^+	$\omega\pi^+$	ωK^0	$\omega\pi^0$
track reconstruction	3.0	3.0	4.0	2.0
\mathcal{R} requirement	2.5	2.6	2.5	3.3
particle identification	1.7	1.7	0.9	0.9
π^0 reconstruction	4.0	4.0	4.0	8.0
K_S^0 reconstruction	—	—	4.9	—
ω mass window	3.0	3.0	3.0	3.0
MC statistics	1.1	1.2	1.8	2.4
signal PDF	$^{+0.1}_{-0.0}$	≤ 0.1	± 0.5	$^{+1.2}_{-0.6}$
$\omega K^+/\omega\pi^+$ feed-across background	$^{+0.3}_{-0.1}$	± 0.3	—	—
$N_{B\bar{B}}$	1.3	1.3	1.3	1.3
Total	6.8	6.8	8.8	9.9

011106 (2006).

- [8] S. Kurokawa and E. Kikutani, Nucl. Instrum. Meth. Phys. Res. Sect. A **499**, 1 (2003), and other papers included in this volume.
- [9] A. Abashian *et al.* (Belle Collab.), Nucl. Instrum. Meth. Phys. Res. Sect. A **479** 117 (2002).
- [10] Y. Ushiroda (Belle SVD2 group), Nucl. Instrum. Meth.

Phys. Res. Sect. A **511**, 6 (2003).

- [11] S. Eidelman *et al.* (Particle Data Group), Phys. Lett. B **592**, 1 (2004).
- [12] We define the thrust axis for a collection of particles as the axis that maximizes the sum of the magnitude of the longitudinal momenta with respect to the axis.
- [13] The Fox-Wolfram moments were introduced in G.C. Fox and S. Wolfram, Phys. Rev. Lett. **41**, 1581 (1978). The Fisher discriminant used by Belle, based on modified Fox-Wolfram moments (SFW), is described in K. Abe *et al.* (Belle Collab.), Phys. Rev. Lett. **87**, 101801 (2001) and K. Abe *et al.* (Belle Collab.), Phys. Lett. B **511**, 151 (2001).
- [14] R. Ammar *et al.* (CLEO Collab.) Phys. Rev. Lett. **71**, 674 (1993). The variable S_{\perp} was first introduced by CLEO in the $B \rightarrow K^*\gamma$ analysis. We use the B thrust axis to calculate S_{\perp} , while CLEO uses the photon direction.
- [15] H. Kakuno *et al.* (Belle Collab.), Nucl. Instr. and Meth. A **533**, 516 (2004).
- [16] J.E. Gaiser *et al.* (Crystal Ball Collab.), Phys. Rev. D **34**, 711 (1986).
- [17] H. Albrecht *et al.* (ARGUS Collab.), Phys. Lett. B **241**, 278 (1990).
- [18] POLE program, v1.0 (<http://www3.tsl.uu.se/~conrad/pole.html>); see also J. Conrad, O. Botner, A. Hallgren, and C. Pérez, Phys. Rev. D **67**, 012002 (2003).
- [19] G.J. Feldman and R.D. Cousins, Phys. Rev. D **57**, 3873, (1998).